BOLETIN DE LA SOCIEDAD ESPAÑOLA DE
Cerámica y Vidrio
www.elsevier.es/bsecv

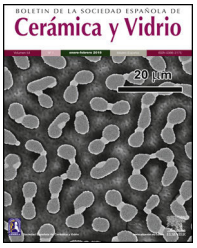

Conductivity and microstructural evaluation of SGDC solid electrolytes synthetized by Pechini and controlled precipitation

*Paola Cristina Cajas Daza, Jorge Luiz de Almeida Ferreira, José Alexander Araujo, José Antônio Euzébio Paiva, Rodrigo Arbey Muñoz Meneses, Cosme Roberto Moreira da Silva**

Department of Mechanical Engineering, Materials Group, University of Brasilia, Brasília, DF 70940-910, Brazil

ARTICLE INFO

Article history:
Received 21 July 2020
Accepted 22 April 2021
Available online 21 May 2021

Keywords:
Synthesis
Pechini
Ceramics
Electrolyte

ABSTRACT

In this work, controlled precipitation synthesis methods and polymeric precursors (Pechini) were used to obtain gadolinium-doped cerium oxide solid electrolytes ($Ce_{0.8}Gd_{0.2}O_{1.9}$) and double-doped cerium oxide with gadolinium and samarium ($Ce_{0.8}Gd_{0.2-x}Sm_xO_{1.9}$ $x = 0.01$; 0.03 and 0.05). The main results indicate that the synthesized powders by the Pechini method present better microstructural characteristics such as larger specific surface area and smaller particle size. Test specimens were compacted (187 MPa) and sintered (1500 °C/6 h) and subsequently characterized. Through the impedance spectroscopy analysis, an increase in the percentage of the samaria caused an increase in the grain boundary and grain conductivity in all the samples under study. In the grain interior, samples without samaria showed heterogeneous regions, where the cation-vacancy pairs are tightly bound, precluding these vacancies from participating in ion conduction. In the samples with samaria, these defect groups are smaller, indicating structural homogeneity, resulting in greater ionic conductivity. Grain boundary specific conductivities show slight increase for samples codoped with samarium oxide. This effect suggests that Sm^{3+} additions change the charge equilibrium in space-charge layer favoring better dopant distribution.

Conductividad y evaluación microestructural de Electrolitos sólidos SGDC sintetizados por Pechini y precipitación controlada

Palabras clave:
Sintesis
Pechini
Cerámica
Electrolitos

RESUMEN

En este trabajo se utilizaron los métodos de síntesis precipitación controlada y precursores poliméricos (Pechini) para obtener electrolitos sólidos de ceria dopada con gadolinio ($Ce_{0.8}Gd_{0.2}O_{1.9}$) y óxido de ceria doblemente dopada con gadolinio y samario ($Ce_{0.8}Gd_{0.2-x}Sm_xO_{1.9}$ $x = 0.01$; 0.03 and 0.05). Los principales resultados indicaron que los

* *Corresponding author.*
E-mail address: cosmeroberto@gmail.com (C.R. Moreira da Silva).
https://doi.org/10.1016/j.bsecv.2021.04.003

polvos sintetizados por el método Pechini presentaron mejores características microestructurales: mayor área de superficie específica y menor tamaño de partícula. Los polvos fueron compactados (187 MPa), sinterizados (1500 °C/6 h) y, por fin, caracterizados. Con análisis de los espectros de impedancia se observó que el aumento del porcentaje de samario provocó aumento de la conductividad del grano y del contorno de grano en todas las muestras en estudio. En el interior del grano las muestras sin samaria mostraron regiones heterogéneas (grupos de defectos) donde pares catión-vacancia están estrechamente unidos, lo que impide su participación en la conducción iónica. En las muestras con samaria, estos grupos de defectos son más pequeños, indicando homogeneidad estructural, obteniendo una conductividad iónica mas alta. La conductividad específica del límite de grano muestra un ligero aumento para las muestras codopadas con óxido de samario. Este efecto sugiere que las adiciones de Sm^{3+} cambian el equilibrio de carga en la capa de carga espacial favoreciendo una mejor distribución del dopante.

Introduction

Solid oxide fuel cells (SOFCs) are electrochemical devices that transform chemical into electrical energy. Hydrogen is used as fuel and oxygen as oxidizing gas. SOFCs consist of two porous electrodes (anode and cathode) and a solid electrolyte. One of the objectives of electrodes is to allow gas to go from the electrode/electrolyte interface and vice versa [1,2]. The wide range of working temperatures is one of the main advantages of SOFCs. This performance depends basically on the materials used in electrolytes and their ability to conduct ions [3]. The materials used in manufacturing these electrolytes are ceramics often with a fluorite structure. Cells are currently manufactured with solid electrolytes based on zirconium oxide and additives, reaching operating temperatures between 800 and 1000 °C. Cerium oxide containing additives has been widely studied for applications with intermediate temperature solid oxide fuel cells (IT-SOFCs), given that this ceramic material reduces the operating temperature of the cell, guaranteeing high performance [4,5]. The choice of doping oxides determines electrolytic conductivity. Previous work [1,6–8] indicated that, in addition to forming vacancies, adding doping cations to the structure favors the formation of large defect groups of vacancy-cation pairs. Electrolyte performance depends on its microstructure and the morphology of the precursor powder. Thus, it is essential to optimize the synthesis methods in order to obtain powders with specific characteristics [9]. The Pechini polymeric precursor process makes it possible to control the stoichiometry and composition of the system, in order to guarantee an atomic-level mixture [10], and is used to obtain a wide range of oxides. The controlled precipitation method for synthesizing is characterized by the precipitation of a solid to a liquid phase. This method makes it possible to control the characteristics of powders produced during the formation of the solid part (nucleation, nucleus growth and saturation) [11], favoring adequate particle size.

Pure cerium oxide (CeO_2) is a mixed conductor because it exhibits both electric and ionic conductivity. However, the ionic conductivity of pure cerium oxide is significantly lower than its electronic counterpart. In order to enhance ionic conductivity in cerium at intermediate temperatures, the addition of lower valent oxides may lead to an increase in vacancy concentration in the structure, making ionic superior to electronic conductivity. It is important that the cations of doping oxides not significantly alter the structure in order to maintain as much stability as possible. The literature [12,13] suggests that the oxides that cause the least distortion, that is, those that contain cations with an ionic radius similar to that of Ce^{+4}, are best suited to doping. Based on these results, gadolinium and samarium oxides were selected in the present study as dopants of CeO_2 to manufacture solid electrolytes.

Omar et al. [14] obtained increase of 30% in bulk conductivity in a codoped system ($Sm_{0.75}Nd_{0.075}Ce_{0.85}O_{2-\delta}$) when compared to undoped $Gd_{0.10}Ce_{0.90}O_{2-\delta}$. In this case, doping with two elements in the same proportions (Sm^{3+} and Nd^{3+}) reached conductivity similar to the obtained previously with Pm3+, at this point, the highest obtained ionic conductivity. Artini et al. [15] carried out double cerium oxide doping using ion with higher ionic radius (Dy^{3+}) and another with smaller radius (Nd^{3+}), aiming to obtain an intermediate radius, similar to the Sm3+. In this case the double doping hinder cluster growth and, as a result, increased the conductivity. In another work [16] Artini et al., 2019 pointed out that for $Ce_{1-x}Gd_xO_{2-x/2}$ systems with doping in a range of $0.10 \leq x < 0.20$, the oxygen vacancies are randomly distributed and free in the crystal lattice, and can contribute to conductive process and are not bind to nano domains. Coles-Aldridge [17] synthetized seven compositions of $Ce_{0.8}Sm_xGd_yNd_zO_{1.9}$ (where x, y and z = 0.2, 0.1, 0.0667 or 0 and $x+y+z=0.2$) using a low temperature method in order to determine the effect of multiple doping on microstructure and conductivity. It was observed an enhancement effect on conductivity for this combination of co-dopants between 300 °C and 700 °C relative to the singly doped compounds – $Ce_{0.8}Sm_{0.2}O$ and $Ce_{0.8}Gd_{0.2}O_{1.9}$.

The present study synthesized ceramic powders from the ($Ce_{0.8}Gd_{0.2-x}Sm_xO_{1.9}$ $x = 0.01$; 0.03 and 0.05) using two different synthesis processes: the Pechini (polymeric precursors) and controlled precipitation methods. Next, the samples were sintered and a comparative analysis was conducted of the ionic conductivity of samples produced from different synthesis methods. Significant differences were found between the ionic conductivity behavior of samples produced with powders

sintered by Pechini and controlled precipitation. Conductivity also increased with a rise in the amount of samaria added. The main novelty of this work was the use of controlled precipitation synthesis methods and polymeric precursors (Pechini) to obtain gadolinium-doped cerium oxide solid electrolytes followed by conductivity determination and diffractometric and microstructural characterization in order to identify the causes of differences in ionic conductivities in samples sintered with powders synthetized with these methods.

Experimental procedure

Powder synthesis

The types of reagents and purity as well as the synthesis method have a significant effect on the desirable characteristics of the product to be obtained. The ceria-based $Ce_{0.8}Gd_{0.2-x}Sm_xO_{1.9}$ systems ($x = 0.01$; 0.03 and 0.05) were obtained using two different synthesis methods: Pechini polymeric precursor and controlled precipitation.

The following reagents were used to obtain the powders in both methods:

- Cerium (III) nitrate hexahydrate (99.5% pure) ($Ce(NO_3)_3{\cdot}6H_2O$)
- Gadolinium nitrate hydrate (99.9% pure) ($Gd(NO_3)_3{\cdot}xH_2O$) $x \sim 6$
- Samarium nitrate hexahydrate (99.9% pure) ($Sm(NO_3)_3{\cdot}6H_2O$).

Synthesis using the Pechini polymeric precursor method was developed using two different solutions (A and B). In solution A, citric acid was dissolved in ethylene glycol at 70 °C with a 1:4 ratio by weight. In solution B, the stoichiometrically calculated precursors of cerium, gadolinium and samarium were dissolved in distilled water, depending on the desired composition. Solutions A and B were mixed to ensure homogenization. Ammonium hydroxide was added to this mixture until the solution reached pH 9. Next, the mixture was heated to 160 °C to evaporate and polymerize the solvent, producing the viscous resin. Finally, the resulting resin was maintained at a temperature of 300 °C for three hours in order to obtain the pre-calcined material.

A solution of water and ethanol at equal proportions (50 ml) was used as a solvent in controlled precipitation, adding ceria nitrate until complete dissolution. Next, gadolinium and samarium nitrates were added at the percentages calculated for each composition. Once the nitrates were dissolved in the solution, the pH was adjusted to 9 by the slow and controlled addition of ammonium hydroxide, thereby guaranteeing the complete formation of precipitates.

Powder characterization

The specific surface area of the powder samples was determined by gas adsorption (BET), which describes the physical adsorption of gases on solid surfaces. The amount of gas adsorbed as a function of pressure at a particular temperature is used to construct the adsorption isotherm [18]. The tests were conducted on micromeritics equipment (ASAP2020).

Laser diffraction particle size analysis of ceria-based powders, obtained by the two synthesis methods, makes it possible to determine the quantitative distribution of particle size and/or sample clusters. For this analysis, the powders were dispersed in ethanol in wet mode. The Horiba LA-930 Laser Scattering Particle Size Distribution Analyzer was used.

Qualitative analysis of the morphology of synthesized powders and assessment of the influence of milling processes on cluster size was conducted by scanning electron analysis. The samples were previously metalized with a thin gold film in order to ensure good surface electrical conductivity and avoid image distortion. The Jeol JSM-7001F scanning electron microscope was used for this analysis.

The microstructure of powders from $Ce_{0.8}Gd_{0.2}O_{1.9}$ and $Ce_{0.8}Gd_{0.15}Sm_{0.05}O_{1.9}$, synthesized by both the Pechini and controlled precipitation methods, were analyzed by high-resolution transmission electron microscopy (HRTEM). The images made it possible to identify the planes in the powder structure. "ImageJ" software was used to measure the distances between the crystallographic planes, resulting in values similar to those found in the interplanar distances of planes (100) and (111) of the characteristic ceria structure.

Electrolyte compaction and sintering

After the synthesis processes, the powders obtained were thermally analyzed to determine the adequate calcination temperature, aimed at eliminating the organic part and volatile elements of the synthesis methods. After this analysis, the thermal treatments of powders obtained by controlled precipitation and those synthesized by the Pechini method were carried out at temperatures between 500 and 550 °C (2 h). Next, high-energy milling of the calcined powders in a ball mill was carried out for one hour at 1000 rpm, using a liquid medium with an ethanol-powder ratio of 5:1. Zirconium balls (2 mm diameter) were used for milling (4:1 ballpowder ratio). After milling, the solution was dried on the heating plate at a temperature of 150 °C, with subsequent sieving (0.046 mm sieve), aimed at uniform particle redistribution. Next, the test specimens were shaped by cold uniaxial pressing in a cylindrical die with a diameter of approximately 10 mm. After compaction, the test specimens of all the compositions were sintered using a two-stage sintering ramp. The initial heating rate was 5 °C/min up to 900 °C with a 5-min plateau, followed by heating up to 1650 °C at a heating rate of 2 °C/min and 5-min plateau, then cooling to a sintering temperature of 1500 °C, maintaining this level for 6 h. The high sintering temperatures were selected based on previous dilatometry, which indicated that these systems exhibit slow kinetics and need high sintering temperature and long plateau times.

Characterization

Sample density was calculated according to ASTM-C744-74, which is based on Archimedes principle [19]. The values obtained make it possible to assess the degree of sample densification and the effects of the calcination and mechanical

milling processes. A SHIMADZU AUY 220 precision balance was used to weigh the sintered test specimens.

Scanning electron microscopy was used for the sintered samples to analyze microstructural homogeneity resulting from the sintering of powders produced by Pechini and controlled precipitation synthesis. The samples analyzed were previously metalized with a thin gold film to ensure good surface electrical conductivity. SEM analyses were performed with a Jeol JSM7001F.

The crystalline phases present in the sintered samples were identified by X-ray diffractometry, using a Shimadzu XRD 6000, with scans between 20° and 80°, in steps of 0.02 degrees/min.

Ionic conductivity was determined with a Solartron SI 1260 Impedance/Gain-Phase Analyzer The measurements were performed in the 1 MHz–1 Hz frequency range with a voltage amplitude of 1000 mV and in the temperature range of 235 °C to 385 °C. The specimen surfaces were ground, polished and sputter coated with conductive gold film using the QUORUM 150R ES equipment, in order to determine ionic conductivity. The Smart v3.3.1 and ZView 2 software were used for data acquisition and to fit the impedance data, respectively.

Samples sintered with powders obtained by the method with the highest ionic conductivity (Pechini) were selected for high-resolution transmission electron microscopy (HRTEM) using the FEI TECNAI G^2 F20 HRTEM microscope. For proper testing, the samples should have specific dimensions compatible with the sample holder. Disks from each of the sintered compositions (3 mm in diameter and 60 μm thick) were obtained. The disks underwent ion-beam thinning until perforation and the formation of extremely thin edges around the hole, transparent to the transmission microscope electron beams. After this preparation, the samples were introduced into HTRM for observation and analyses.

Results and discussion

Characterization of ceramic powders

The characterizations of synthetized powders were carried out without calcination and milling.

Specific surface area

The specific surface areas of the synthetized powders, obtained using the Brunauer–Emmett–Teller (BET) technique shown in Table 1, exhibit values of up to 44 m^2/g in the powders synthetized by the Pechini method. Powders produced by controlled precipitation showed much lower values (approximately 16 m^2/g). The higher specific surface areas observed in Pechini synthesis is expected to result in better reactivity between particles during the sintering process, thereby, possible decreasing the temperature needed for densification. This effect minimized imperfections such as the presence of pores, impurity segregation to the boundary regions which promotes expansion of the crystalline lattice and formation of microcracks [20]. No large variations in the surface area of particles were observed with changes in the codoped compositions. However, significant variations in these areas were found for the different synthesis methods.

Table 1 – Specific surface area of synthetized powders.

Powder composition	Specific surface area (m^2/g)	
	Controlled precipitation	Pechini
$Ce_{0.80}Gd_{0.20}O_{1.9}$	5.10 ± 0.13	40.15 ± 0.02
$Ce_{0.80}Gd_{0.19}Sm_{0.01}O_{1.9}$	10.03 ± 0.14	41.99 ± 0.018
$Ce_{0.80}Gd_{0.17}Sm_{0.03}O_{1.9}$	10.92 ± 0.09	36.38 ± 0.78
$Ce_{0.80}Gd_{0.15}Sm_{0.05}O_{1.9}$	16.74 ± 0.37	44.32 ± 0.22

Particle size analysis

Laser diffraction particle size analysis of synthetized powders makes it possible to determine particle size and/or cluster distribution. Fig. 1(A) exhibits the particle size distribution of the $Ce_{0.8}Gd_{0.19}Sm_{0.01}O_{1.9}$ sample obtained using the controlled precipitation method, observing clusters with bimodal size distribution and dimensions of 8.8 and 2.35 μm. Fig. 1(B) exhibits this distribution for a system of the same composition, but synthesized using the Pechini method. In this case, the maximum cluster sizes are smaller (between 0.299 and 1.95 μm). Based on these results, it can be inferred that powders synthetized by the controlled precipitation method formed strong, large and difficult to disaggregate clusters.

Scanning electron microscopy analyses of the synthetized powders

Fig. 2 presents the micrographs of $Ce_{0.8}Gd_{0.19}Sm_{0.01}O_{1.9}$ powders obtained using the controlled precipitation (2(A)) and Pechini methods (2(B)), respectively. Micrographs made it possible to qualitatively observe that the powders obtained by controlled precipitation exhibit larger clusters than those syn-

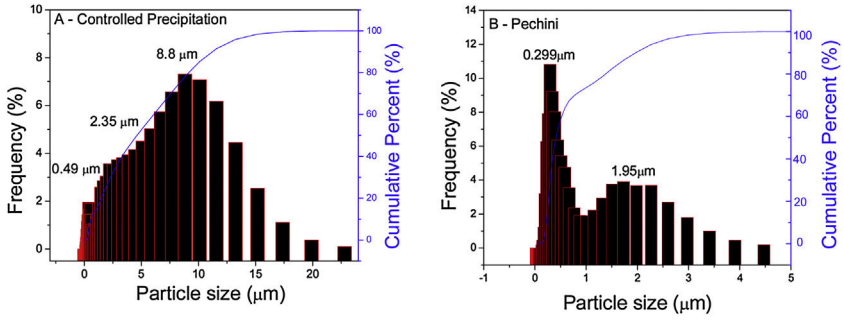

Fig. 1 – Particle size distribution of $Ce_{0.80}Gd_{0.19}Sm_{0.01}O_{1.9}$ powders using the controlled precipitation (A) and Pechini (B) methods.

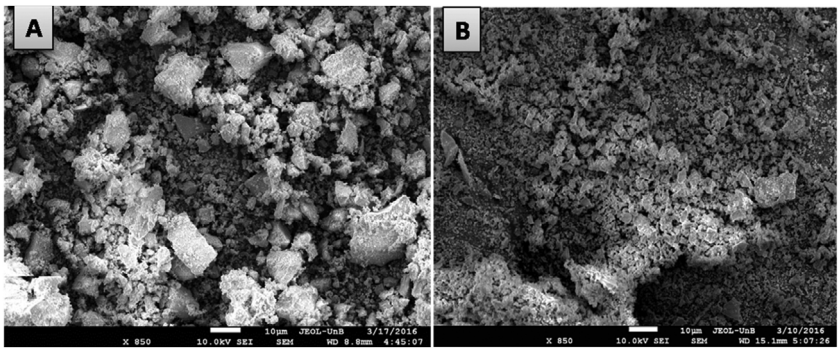

Fig. 2 – SEM micrograph of $Ce_{0.80}Gd_{0.19}Sm_{0.01}O_{1.9}$ powders synthetized by the controlled precipitation (A) and Pechini (B) methods.

thesized by the Pechini method. These results are compatible with particle size analyses presented in Fig. 1(A) and (B). The same effect was observed in the other compositions prepared here.

The morphological characterizations of the powders demonstrate that the Pechini method favors powders with smaller particle sizes/clusters. The powders synthetized by the Pechini method exhibited a larger specific surface area, that is expected to favor the compaction and sintering processes, maximizing density and minimizing the presence of pores that act as an insulating phase, directly affecting ionic conductivity in the grain boundaries.

High-resolution transmission electronic microscopy of the synthetized powders

The microstructures of powders from the $Ce_{0.8}Gd_{0.2}O_{1.9}$ and $Ce_{0.8}Gd_{0.15}Sm_{0.05}O_{1.9}$ compositions synthesized by the Pechini and controlled precipitation methods were examined by high-resolution transmission electron microscopy (HRTEM). "ImageJ" software was used to measure the distances between crystalline planes, resulting in values similar to those found in the interplanar distances of planes (100) and (111) of the characteristic ceria structure. Figs. 3 and 4 present the microstructural analyses of Ce0.8Gd0.2O1.9 powders (without codoping), obtained by the controlled and Pechini methods, respectively. Fig. 3A shows the crystalline planes of the particles. In the enlargements of two different zones presented in Fig. 3B, the spacings between these planes were measured, obtaining 0.301 nm and 0.256 nm, corresponding to the interplanar distances of planes (111) and (100), respectively, of the ceria structure [21].

Fig. 4A presents the crystalline lattice of ultrathin particles. Fig. 4B shows the enlargement of two zones of interest from Fig. 4A, demonstrating crystalline lattice spacings, with values of 0.297 and 0.303 nm, near the interplanar distances of plane (111) of the fluorite structure of cerium oxide.

Selected area electron diffraction (SAED) patterns make it possible to study crystalline lattice symmetry and calculate interplanar distances, allowing phase identification. The images in Figs. 3C and 4C present the SAED pattern of Ce0.8Gd0.2O1.9 powders obtained by the controlled precipitation and Pechini methods, respectively, showing the presence of concentric rings characteristic of polycrystalline systems. The electron diffraction patterns identified diffraction rings corresponding to reflection planes (100), (200), (220) and (311). The images are compatible with the cubic arrangement characteristic of cerium oxide (PDF-34-0394).

Figs. 5 and 6 exhibit HRTEM microstructural analyses of samaria-codoped and $Ce_{0.8}Gd_{0.15}Sm_{0.05}O_{1.9}$ powders obtained by the controlled precipitation and Pechini methods, respectively.

In the enlargements of the images of Fig. 5B, the lattice spacings presented values of 0.297 and 0.259, corresponding to the interplanar distances of planes (111) and (100) of the cubic structure of ceria. Likewise, the interplanar distances in Fig. 6B were 0.298 and 0.254 in relation to the interplanar distances of planes (111) and (100) of the cubic structure of ceria [21]. Figs. 5C and 6C present the SAED patterns for samaria-doped powders synthesized by the two methods used here.

Characterization of sintered samples

Density

Table 2 shows the relative densities of the sintered samples, produced from powders synthesized by different methods. The densities of the samples sintered from powders synthesized by controlled precipitation are lower, with values between 83 and 87% of theoretical density. These low densities are associated with the morphological properties generated in this synthesis process, such as the low specific surface area and large cluster size, resulting in low sinterability. The densities of the solid electrolytes obtained from the powders synthesized by the Pechini method are higher (94–96% of theoretical density), within the adequate electrolyte manufacturing range [19].

Scanning electron microscopy of the sintered samples

The differences in density results for samples sintered from ceramic powders produced by different synthesis methods were confirmed by scanning electron microscopy images. Fig. 7 shows test specimen micrographs of $Ce_{0.8}Gd_{0.19}Sm_{0.01}O_{1.9}$ sintered with powders obtained by controlled precipitation (A) and the Pechini method (B). The controlled precipitation sample exhibits a heterogeneous microstructure and high porosity, while that obtained by the Pechini method displayed a homogeneous microstructure

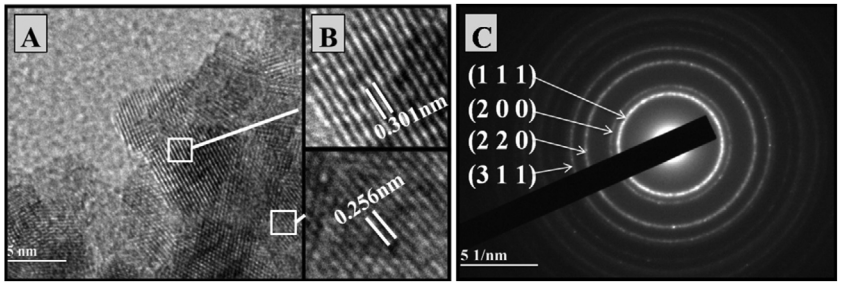

Fig. 3 – HRTEM images of $Ce_{0.80}Gd_{0.20}O_{1.9}$ powder (without codoping) synthesized by controlled precipitation, showing the planes of the crystalline lattice (A), interplanar distances (B) and diffraction rings (C).

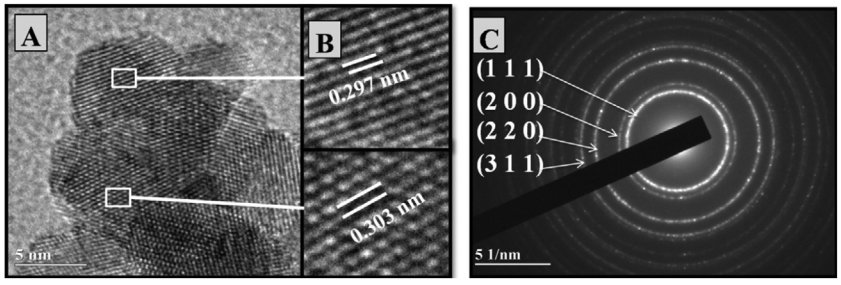

Fig. 4 – HRTEM images of the $Ce_{0.80}Gd_{0.20}O_{1.9}$ powders (without codoping) synthesized by Pechini with crystallographic planes (A), interplanar distances (B) and diffraction rings (C).

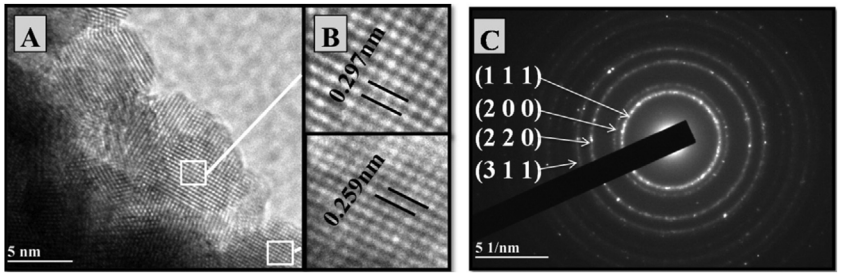

Fig. 5 – HRTEM of the $Ce_{0.80}Gd_{0.15}Sm_{0.05}O_{1.9}$ powder (codoped) synthesized by controlled precipitation with the crystallographic planes (A), interplanar distances (B) and diffraction rings (C).

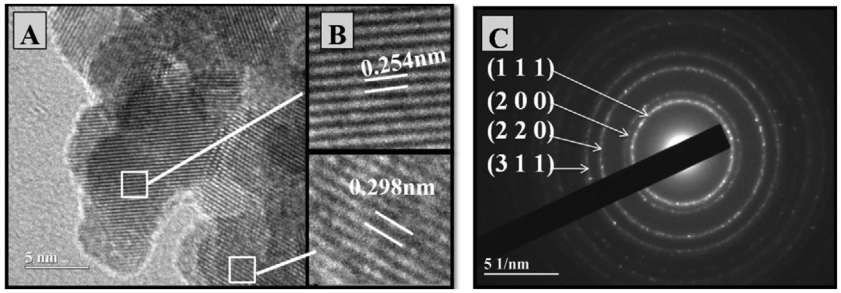

Fig. 6 – HRTEM of $Ce_{0.80}Gd_{0.15}Sm_{0.05}O_{1.9}$ powder (codoped) synthesized by the Pechini method with the crystallographic planes (A), interplanar distances (B) and diffraction rings (C).

Table 2 – Relative densities (%) of samples sintered from powders synthesized by the controlled precipitation and Pechini methods.

Sintered composition	Controlled precipitation	Pechini
$Ce_{0.8}Gd_{0.2}O_{1.9}$	81.45 ± 0.35	94.22 ± 0.12
$Ce_{0.8}Gd_{0.19}Sm_{0.01}O_{1.9}$	86.52 ± 0.43	96.00 ± 0.49
$Ce_{0.8}Gd_{0.17}Sm_{0.03}O_{1.9}$	86.56 ± 0.25	96.61 ± 0.23
$Ce_{0.8}Gd_{0.15}Sm_{0.05}O_{1.9}$	86.13 ± 0.39	96.17 ± 0.32

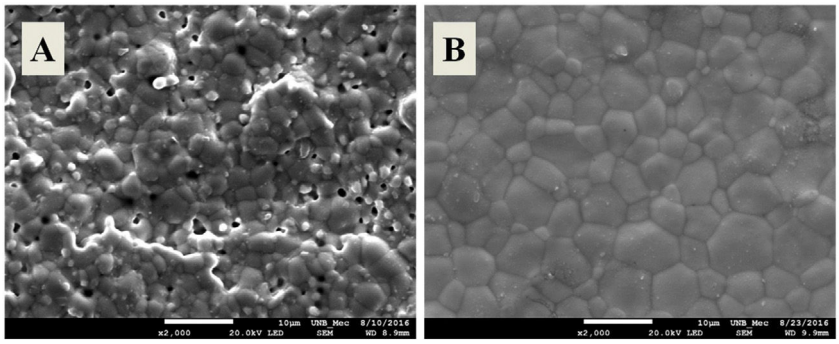

Fig. 7 – Scanning electron microscopy of the $Ce_{0.80}Gd_{0.19}Sm_{0.01}O_{1.9}$ sample sintered from the powders obtained by controlled precipitation (A) and the Pechini method (B).

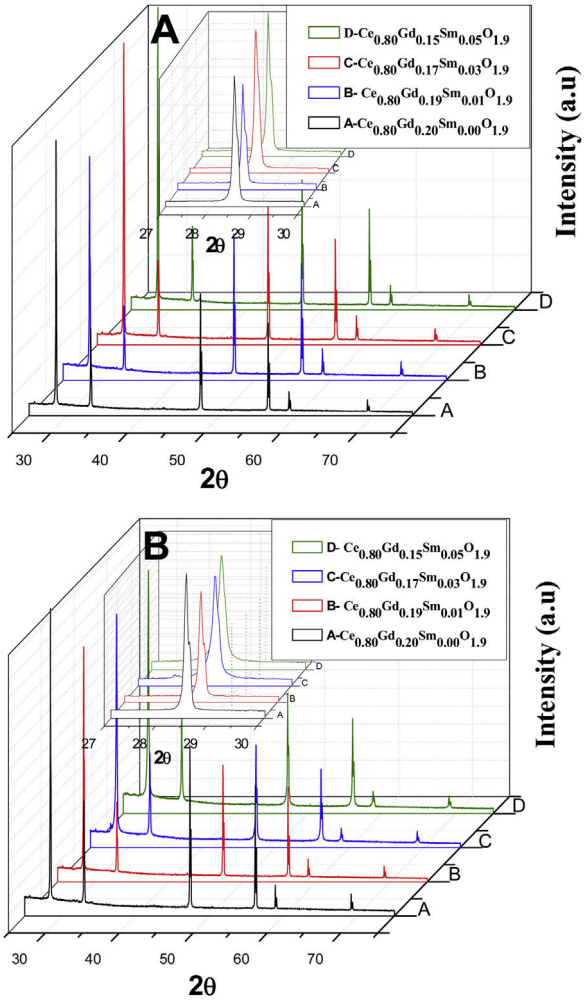

Fig. 8 – X-ray diffractograms of electrolytes sintered from powders synthesized by the controlled precipitation (A) and Pechini (B) methods.

with low porosity. The other compositions produced here showed similar behavior.

X-ray diffractometry

The diffractograms of Fig. 8, corresponding to all the compositions analyzed in the present study, that is, the

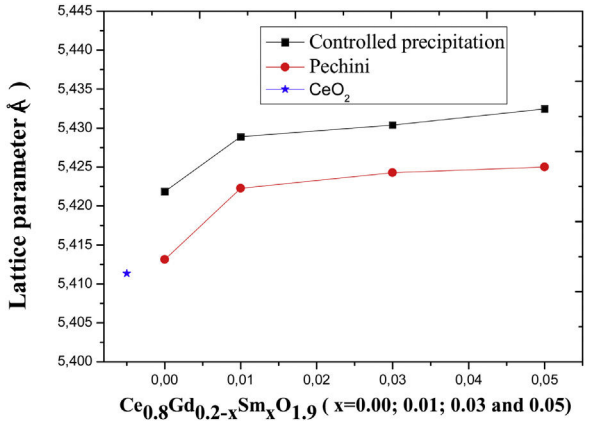

Fig. 9 – Variation in lattice parameters with the synthesis method and electrolyte composition.

$Ce_{0.8}Gd_{0.2-x}Sm_xO_{1.9}$ systems (x = 0.00; 0.01; 0.03 and 0.05) sintered with powders synthesized by the controlled precipitation (A) and Pechini (B) methods, contain the cubic fluorite phase, exhibiting the main cerium oxide diffraction peaks (PDF 34-0394) [22]. The presence of a single phase in the diffractograms suggests that the doping oxides entered the solid solution in the structure of CeO_2. The diffractograms display the cubic fluorite phase in all the samples, although small displacements are observed in the diffraction peaks with a variation in composition, with no structural deformations. Changes in the angles corresponding to the diffractogram peaks are caused by replacing cerium atoms with Sm3+ and Gd3+ atoms, thereby varying the lattice parameters for each composition.

The lattice parameter of the CeO_2 is 0.5411 nm [23]. In order to assess changes in CeO_2 structure with the addition of the dopants used here, diffractogram data presented in Fig. 8 were used. These data were used to calculate the lattice parameters of the sintered samples, where a peak value of 2θ was used to calculate the interplanar distance based on Bragg's law [24]. Fig. 9 presents the variation in the lattice parameter with an increase in codoping content for the different powder synthesis methods. For $Ce_{0.8}Gd_{0.2}O_{1.9}$, the lattice parameter found is 0.5413 nm for the system obtained by the Pechini method and 0.5422 for that obtained by controlled precipitation doped with higher lattice parameters, showing that this synthesis

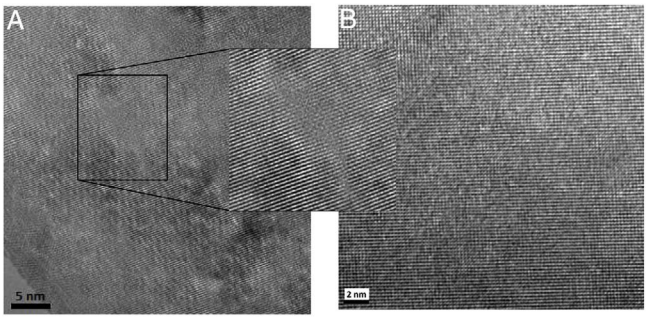

Fig. 10 – HRTEM images of systems obtained by the Pechini method of $Ce_{0.8}Gd_{0.2}O_{1.9}$ (without codoping) with light-colored regions characteristic of defect concentration in the crystalline lattice (A) and $Ce_{0.8}Gd_{0.15}Sm_{0.05}O_{1.9}$ (with codoping) with smaller concentrations of these defects (B).

process promotes greater distortion in the crystalline lattice, which has a harmful effect on the ionic conduction of these systems.

The powders synthesized by the Pechini method exhibit lattice parameters closer to those of cerium oxide, thereby causing fewer crystalline distortions.

High-resolution transmission electron microscopy of the sintered samples

HRTEM of the grain interiors. Given the low total conductivity of samples sintered with powders produced by controlled precipitation synthesis, only HRTEM assessment of the grain interiors of samples with high total conductivity was conducted; that is, only those sintered from powders produced by the Pechini synthesis method. In this analysis, we sought to identify the causes of increased grain conductivity as a function of the rise in codoping with samaria. Fig. 10 presents HRTEM grain images of systems obtained by the Pechini method, the composition doped only with gadolinium ($Ce_{0.8}Gd_{0.2}O_{1.9}$) and that doped with gadolinium and codoped with samaria ($Ce_{0.8}Gd_{0.15}Sm_{0.05}O_{1.9}$). These images show regions containing brightly colored atoms, indicating small distortions in the crystalline lattice that may be associated with small defects caused by the addition of dopants. The image in Fig. 10A, corresponding to the system without samaria codoping ($Ce_{0.8}Gd_{0.2}O_{1.9}$), exhibits different regions of the matrix, where the atoms show no definite order, thereby confirming the presence of large ordered defect clusters (nanodomains). In the images of Fig. 10B, corresponding to the samaria-codoped system, the atoms displayed better structural uniformity, which is repeated in long atomic distances.

The HRTEM images show the effectiveness of samaria codoping in obtaining systems with higher structural homogeneity. These studies, conducted with high-resolution transmission electron microscopy, identified the presence of nanodomains in both electrolytes (with and without samaria codoping), exhibiting a marked predominance of these defects in the system without samaria. These nanodomains are responsible for the high grain resistivity in these noncodoped samples, since the charge carriers are blocked in these regions. The oxygen vacancies in the non-codoped samples are tightly bound to the doping cations, remaining immobilized [25], hindering effective O^{-2} ion conduction through the structure and directly affecting the ionic conductivity of these systems not codoped with samaria.

Ionic conductivity

Fig. 11 shows impedance spectra, known as Nyquist diagrams, for samples tested at 310 °C. Points A, B and C in this figure show regions of low, medium and high frequencies, respectively. For all samples, two semicircles are clearly observed, related to ionic contribution of grain interior (high frequencies) and grain boundary (intermediate frequencies) [26]. A third incomplete semicircle at low frequencies could be, presumably, correlated to charge carriers (O^{-2}) blocking at the interface sample/electrode. This behavior is indicative that samples evaluated in this work reveal ionic conductivity.

The impedance values obtained in the impedance spectra for each testing temperature were multiplied by the geometric factor of each sample (A/l, where l is the thickness and A the sample area) to obtain the Nyquist plots given in Fig. 11. Therefore, the intercept between each circle (high and low frequencies) and the real axis (Z') of diagram of impedance represent, respectively, bulk and grain boundary contribution to the resistivity of the sample. Samples of the same composition ($Ce_{0.80}Gd_{0.15}Sm_{0.05}O_{1.9}$) and originated from different synthesis methods showed different grain interior resistivity, reaching 250 kΩ cm for Pechini and 480 kΩ cm for controlled precipitation. These results are indicative that Pechini method favors sintering samples with higher densities and, therefore, with lower bulk resistivity. In this case, the charge carriers in samples with high densities travel shorter effective lengths than in porous samples. In this later case (porous samples), charger carrier needs to travel longer path, and overcome porosities to produce an effective ionic conductivity.

Fig. 12 shows logarithms of grain interior and grain boundary conductivity plotted against the inverse of temperature (Arrhenius graphic) [27]. to observe the temperature dependence of conductivity. Previous work [28] revealed that the specific conductivity of grain boundary is related to the effective grain boundaries area taking part in the conduction process.

To obtain the specific conductivity of grain boundary (σ_{CG}^{Esp}) it was used the inverse of the contribution of grain boundary resistivity $\left(\frac{1}{PCG}\right)$ times the average thickness of grain boundary (D) divided by the grain size (TG) $\left(\sigma_{CG}^{Esp} = \frac{1}{PCG} * \frac{D}{TG}\right)$, as related in previous work [2], for each test temperature. According to literature [26] and considering the "brickwork" model. The ratio between grain capacitance (C_g) and grain boundary (C_{gb}) is correlated to dimensionless microstructural parameter between grain boundary thickness (D) and grain size (TG). Therefore it can be approximated the relation $C_g/C_{gb} = D/TG$. The obtained capacitances values, using the software Zview for all samples reached the approximated values of 3×10^{-11} F and 3×10^{-8} F for electric contribution of grain and grains boundary respectively, reaching values of ratio C_g/C_{gb} of approximately 0.001 in this work.

As depicted in Fig. 12(A and C), the controlled increase of co-dopant (Samarium oxide) causes the grain interior conductivity increase for samples obtained from Pechini powders.

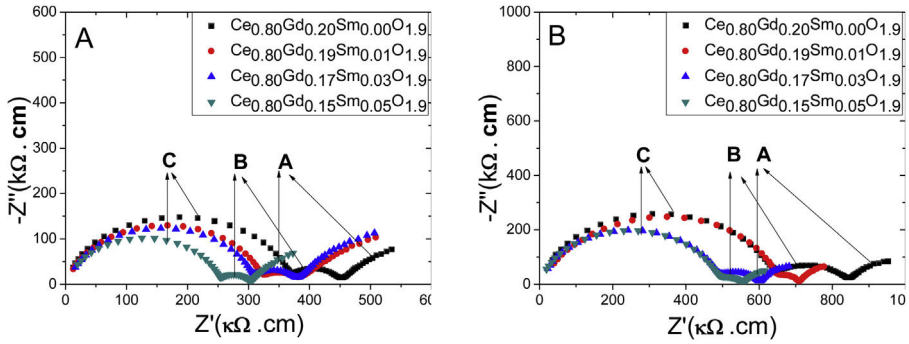

Fig. 11 – Nyquist plots of electrolytes with powders synthesized by (A) Pechini method and (B) controlled precipitation at 583 K.

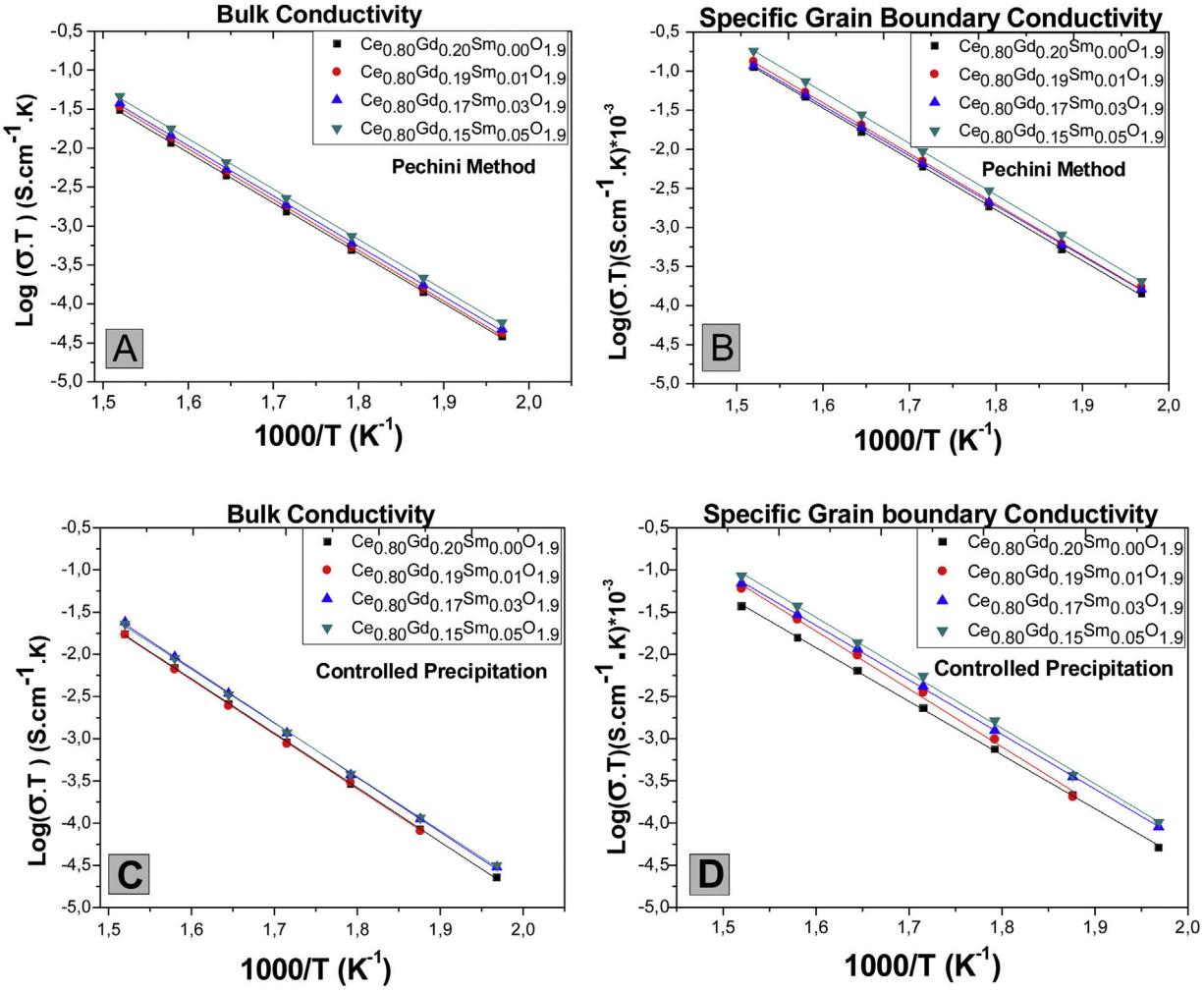

Fig. 12 – Arrhenius plots of grain conductivity and of specific grain boundary conductivity for sintered samples obtained with powder synthetized by the Pechini method (A and B) and controlled precipitation (C and D).

However, this behavior is not clearly observed for samples obtained with controlled precipitation. In systems doped with cerium oxides, such as those in the present work, the possible creation of nanodomains in grain interiors could reduce the ionic conductivity of this material [29]. In the present work it was experimentally observed that the ionic conductivity increases with samarium oxide addition. Therefore, it is suggested that additions of small amount of a second dopant, without compound stoichiometry alteration, favors local cation ordering and oxygen holes in grain interior, favoring mobility of charge carriers and, as result, increasing ionic conductivity.

Table 3 – Total conductivity $\times 10^{-2}$ S.cm^{-1} as a function of the temperature of systems obtained by the Pechini and controlled precipitation methods.

Sintered composition		385 °C	500 °C	600 °C	700 °C
Total conductivity $\times 10^{-2}$ S.cm (Pechini)					
1.	$Ce_{0.8}Gd_{0.2}O_{1.9}$	0.00366	0.086	0.691	3.576
2.	$Ce_{0.8}Gd_{0.19}Sm_{0.01}O_{1.9}$	0.00408	0.099	0.808	4.224
3.	$Ce_{0.8}Gd_{0.17}Sm_{0.03}O_{1.9}$	0.00434	0.101	0.805	4.138
4.	$Ce_{0.8}Gd_{0.15}Sm_{0.05}O_{1.9}$	0.00561	0.133	1.078	5.614
Total conductivity $\times 10^{-2}$ S.cm (Controlled Precipitation)					
1.	$Ce_{0.8}Gd_{0.2}O_{1.9}$	0.00181	0.0427	0.337	1.722
2.	$Ce_{0.8}Gd_{0.19}Sm_{0.01}O_{1.9}$	0.00202	0.0522	0.434	2.302
3.	$Ce_{0.8}Gd_{0.17}Sm_{0.03}O_{1.9}$	0.00272	0.0649	0.522	2.706
4.	$Ce_{0.8}Gd_{0.15}Sm_{0.05}O_{1.9}$	0.00275	0.0637	0.504	2.571

Fig. 12(B and D) show Arrhenius graphics for specific conductivities of grain boundaries (σ_{CG}^{Esp}). In terms of codoping, the grain boundaries of an ionic conductor like cerium oxide doped with gadolinium oxide are composed of the nucleus of the boundary with positive charge and two adjacent space charge layers with negative charge [31]. Structurally, the space charge layers are part of the grain (crystallographically equal to the grains), but electrically part of the grain boundaries [30]. Particularly in cerium oxide, it was experimentally observed that the trivalent solute such as gadolinium would be also segregated at the space charge layer of grain boundary and not only in the nucleus [30,31] giving rise to low mobility of charge carriers in this zone and, therefore, increasing its resistivity. For the systems obtained in this work, Fig. 12(B) and (D) show that grain boundary specific conductivities show slight increase for samples codoped with samarium oxide. This effect suggests that Sm^{3+} additions change the charge equilibrium in space-charge layer [31] favoring better dopant distribution. The vacancies generated by these dopants will have active participation in the conductive process.

Total conductivity as a function of temperature shown in Table 3 confirms the thermally activated behavior of these systems. The rise in test temperature increases ionic conductivity in all the cases. The samples prepared with the powders obtained by the Pechini method exhibited the highest conductivity values obtained in any condition, particularly in $Ce_{0.8}Gd_{0.15}Sm_{0.05}O_{1.9}$.

The results obtained in HRTEM analyses demonstrate that the electrolytes produced with powders synthesized with the Pechini method and greater additions of samaria exhibit better structural homogeneity, with low concentrations of nanodomains responsible for the entrapment of O^{-2} vacancies. Thus, an increase in samaria promotes higher ionic conductivities, results compatible with the differences identified in the conductivity of $Ce_{0.8}Gd_{0.20}O_{1.9}$ and $Ce_{0.8}Gd_{0.15}Sm_{0.05}O_{1.9}$ samples presented in Table 3.

Conclusions

The Pechini method made it possible to obtain powders with a large surface area, lower particle size distribution and weak, easy-to-disaggregate clusters, when compared to powders sintered by controlled precipitation. These characteristics of Pechini powders enable better reactivity between the particles during sintering, resulting in better compacted powder densities, reaching a relative density of approximately 96%.

The presence of a single phase in the diffractograms suggests that doping oxides entered the solid solution in the structure of CeO_2. Crystalline lattice spacings showed values near those of interplanar distances in the fluorite structure of cerium oxide, demonstrating the formation of the compound in the syntheses.

Ionic conductivity of the grain interior and grain boundary of the samples exhibited a dependence on the synthesis method and codoping with samaria. In the grain interior, samples without samaria showed heterogeneous regions where the cation-vacancy pairs are tightly bound, precluding these vacancies from participating in ion conduction. In the samples with samaria, these defect groups are smaller, indicating structural homogeneity, resulting in greater ionic conductivity.

Grain boundary specific conductivities show slight increase for samples codoped with samarium oxide. This effect suggests that Sm^{3+} additions change the charge equilibrium in space-charge layer [31] favoring better dopant distribution. The vacancies generated by these dopants will have active participation in the conductive process.

With respect to density, the higher grain boundary conductivity in the samples produced with Pechini powders is related, for a same composition, to the minimal porosity, since porosity acts as an insulating phase.

The ionic conductivity of samaria-codoped ceria can be changed by the synthesis method due primarily to its influence on the morphology of the resulting powders, particle size distribution, final density of the sintered material and porosity in the compacted powders, resulting in systems with the same composition, but different conducting properties.

REFERENCES

[1] F. Ye, A. Toshiyuki Mori, D.R. Ou, B.C. Jin Zou, J. Drennan, A structure model of nano-sized domain in Gd-doped ceria, Solid State Ionics 180 (2009) 1414–1420.
[2] A.B. Stambouli, E. Traversa, Renew. Sustain. Energy Rev. 6 (2002) 433.
[3] G.N. Prodromidis, F.A. Coutelieris, Solid oxide fuel cell systems for electricity generation: an optimization prospect, Renew. Energy 146 (2020) 38–43.

[4] K. Eguchi, Ceramic materials containing rare earth oxides for solid oxide fuel cell, J. Alloys Compd. 250 (1–2.) (1997) 486–491.
[5] A. Moure, J. Tartaj, C. Moure, Synthesis, sintering and electrical properties of yttria-calcia-doped ceria, J. Eur. Ceram. Soc. 29 (12) (2009) 2559–2565.
[6] S. Singhal, K. Kendall, High temperature solid oxide fuel cells: fundamentals, Des. Appl. (2002).
[7] F. Ye, D.R. Ou, T. Mori, Microstructural evolution in a CeO2-Gd2O3 system, Microsc. Microanal. 18 (1) (2012) 162–170.
[8] P.C.C. Daza, R.A.M. Meneses, A.C.M. Rodrigues, C.R.M. da Silva, Ionic conductivities and high resolution microscopic evaluation of grain and grain boundaries of cerium-based codoped solid electrolytes, Ceram. Int. 44 (12) (2018) 13699–13705.
[9] N. Cioatera, V. Pârvulescu, A. Rolle, R.N. Vannier, Enhanced ionic conductivity of Sm, Gd-doped ceria induced by modification of powder synthesis procedure, Ceram. Int. 38 (7) (2012) 5461–5468.
[10] E.C. Grzebielucka, A.S.A. Chinelatto, S.M. Tebcherani, A.L. Chinelatto, Synthesis and sintering of Y2O3-doped ZrO2 powders using two Pechini-type gel routes, Ceram. Int. 36 (July (5)) (2010) 1737–1742.
[11] C.V.R. Madroñero, J.E.R. Paéz, Sodium aluminates obtained from the Al(NO3)3 • 9H2O – NaOH system using the controlled precipitation method, Ing. Investig. 30 (2) (2010) 16–24.
[12] H. Inaba, H. Tagawa, Ceria-based solid electrolytes, Solid State Ionics 83 (1–2) (1996) 1–16.
[13] J. Prado-Gonjal, R. Schmidt, J. Espíndola-Canuto, P. Ramos-Alvarez, E. Morán, Increased ionic conductivity in microwave hydrothermally synthesized rare-earth doped ceria Ce1−xRExO2−(x/2), J. Power Sources 209 (July) (2012) 163–171.
[14] S. Omar, E.D. Wachsman, J.C. Nino, Higher conductivity Sm3+ and Nd3+ co-doped ceria-based electrolyte materials, Solid State Ionics 178 (2008) 1890–1897.
[15] C. Artini, L. Gigli, M.M. Carnasciali, M. Pani, Effect of the (Nd Dy)-double doping on the structural properties of ceria, Inorganics 7 (2019) 94.
[16] C. Artini, et al., Transport properties and high temperature Raman features of heavily Gd-doped ceria, Energies 12 (2019) 4148.
[17] V.A. Coles-Aldridge, R.T. Baker, Ionic conductivity in multiply substituted ceria-based electrolytes, Solid State Ionics 316 (2018) 9–19.
[18] M. Rezaei, S.M. Alavi, S. Sahebdelfar, Z.-F. Yan, Tetragonal nanocrystalline zirconia powder with high surface area and mesoporous structure, Powder Technol. 168 (October (2)) (2006) 59–63.
[19] A. Arabac, M.F. Öksüzömer, Preparation and characterization of 10mol% Gd doped CeO 2 (GDC) electrolyte for SOFC applications, Ceram. Int. 38 (8) (2012) 6509–6515.
[20] J.L. Narváez-semanate, J.J. Cabrera, R.A. Vargas-zapata, J.E. Rodríguez-páez, Obtención de nanopartículas de zro2 dopado con y2o3 utilizando rutas químicas, Rev. Latinoam. Metarlugia Mater. 27 (2) (2007) 124–134.
[21] P.S. Murphin Kumar, et al., Pt nanoparticles supported on mesoporous CeO2 nanostructures obtained through green approach for efficient catalytic performance toward ethanol electro-oxidation, ACS Sustain. Chem. Eng. 5 (12) (2017) 11290–11299.
[22] E.N.S. Muccillo, et al., Propriedades físicas do óxido de cério preparado por técnica de solução e a condutividade elétrica em função da pressão parcial de oxigênio em cerâmicas sinterizadas, Cerâmica 51 (2005) 157–162.
[23] Z. Tianshu, P. Hing, H. Huang, J. Kilner, Ionic conductivity in the CeO2-Gd2O3 system (0.05≤Gd/Ce≤0.4) prepared by oxalate coprecipitation, Solid State Ionics 148 (3–4) (2002) 567.
[24] D. Sarkar, D. Mohapatra, S. Ray, S. Bhattacharyya, S. Adak, N. Mitra, Synthesis and characterization of sol–gel derived ZrO2 doped Al2O3 nanopowder, Ceram. Int. 33 (September (7)) (2007) 1275–1282.
[25] D.R. Ou, F. Ye, T. Mori, Defect clustering and local ordering in rare earth codoped ceria, Phys. Chem. Chem. Phys. 13 (20) (2011) 9554–9560.
[26] J.T.S. Irvine, D.C. Sinclair, A.R. West, Electroceramics: characterization by impedance spectroscopy, Adv. Mater. 2 (March (3)) (1990) 132–138.
[27] C. Zhang, C.-J. Li, G. Zhang, X.-J. Ning, C.-X. Li, H. Liao e, C. Coddet, Ionic conductivity and its temperature dependence of atmospheric plasma-sprayed yttria stabilized zirconia electrolyte, Mater. Sci. Eng. B (2007) 24–30.
[28] D.P.F. De Souza, M.F. De Souza, Liquid phase sintering of RE2O3: YSZ ceramic Part II grain boundary electrical properties, J. Mater. Sci. 34 (June) (1999) 6107–6114.
[29] R.M. Kasse, J.C. Nino, Ionic conductivity of SmxNdyCe0.9O2−δ codoped ceria electrolytes, J. Alloys Compd. 575 (2013) 399–402.
[30] X. Guo, R. Waser, Electrical properties of the grain boundaries of oxygen ion conductors: acceptor-doped zirconia and ceria, Prog. Mater. Sci. 51 (2) (2006) 151–210.
[31] C. Kjølsetha, H. Fjeld, Ø. Prytz, P.I. Dahl, C. Estournès, R. Haugsrud, T. Norb, Space–charge theory applied to the grain boundary impedance of proton conducting BaZr0.9Y0.1O3, Solid State Ionics 181 (n 5–7) (2010) 268–275, 0167-2738.